Supplement of Atmos. Chem. Phys., 22, 8073–8096, 2022
https://doi.org/10.5194/acp-22-8073-2022-supplement

Atmospheric Chemistry and Physics
Open Access

Supplement of

Chemical properties, sources and size-resolved hygroscopicity of submicron black-carbon-containing aerosols in urban Shanghai

Shijie Cui et al.

Correspondence to: Xinlei Ge (caxinra@163.com)

Table S1: Summary of the input parameters and uncertainties (±σ) for the calculations of hygroscopic parameters.

Parameter	average values	Uncertainty	Reference
O/C	0.26	±0.06	Measured from SP-AMS
κ_{AN}	0.58	±0.01	Gysel et al., (2007)
κ_{AS}	0.48	±0.01	Gysel et al., (2007)
κ_{AHS}	0.56	±0.01	Gysel et al., (2007)
κ_{OA} / (O / C)	0.29	±0.05	Chang et al.,(2010)
$\kappa_{rBC\text{-}rich}$	0.09	±0.02	Chang et al.,(2010)
$\kappa_{HOA\text{-}rich}$	0.02	±0.01	Chang et al.,(2010)
κ_{BBOA}	0.03	±0.01	Chang et al.,(2010)
$\kappa_{WS\text{-}HOA}$	0.09	±0.02	Chang et al.,(2010)
$\kappa_{LO\text{-}OOA}$	0.07	±0.01	Chang et al.,(2010)
$\kappa_{MO\text{-}OOA}$	0.16	±0.03	Chang et al.,(2010)
κ_{rBC}	0		
ε_{AN}	0.192	±0.083	Wu et al., (2016)
ε_{AS}	0.089	±0.064	Wu et al., (2016)
ε_{AHS}	0.024	±0.016	Wu et al., (2016)
$\varepsilon_{rBC\text{-}rich}$	0.089	±0.043	Wu et al., (2016)
$\varepsilon_{HOA\text{-}rich}$	0.099	±0.065	Wu et al., (2016)
ε_{BBOA}	0.044	±0.034	Wu et al., (2016)
$\varepsilon_{WS\text{-}HOA}$	0.104	±0.083	Wu et al., (2016)
$\varepsilon_{LO\text{-}OOA}$	0.071	±0.046	Wu et al., (2016)
$\varepsilon_{MO\text{-}OOA}$	0.115	±0.066	Wu et al., (2016)
ε_{rBC}	0.196	±0.069	Wu et al., (2016)

Table S2: Summary of correlation coefficients between different *r*BCc OA factors and NR-PM$_1$ OA factors with the ship emission tracer (V) during ship emission period (SEP) and non-ship emission period (Non-SEP)(see main text for details), respectively.

		*r*BCc OA								NR-PM$_1$ OA			
	r	*r*BC	HOA-rich	*r*BC-rich	BBOA	WS-HOA	LO-OOA$_{rBC}$	MO-OOA$_{rBC}$	HOA$_{rBC}$	HOA	COA	LO-OOA$_{NR\text{-}PM1}$	MOOOA $_{NR\text{-}PM1}$
SEP	V	0.69	0.69	0.28	0.55	0.72	0.22	-0.15	0.71	0.84	0.08	0.64	0.02
No-SEP	V	-0.01	0.25	0.01	-0.01	-0.04	-0.15	-0.62	0.06	0.19	0.20	-0.26	-0.77

Figure S1: Location of the sampling site (red five-pointed star) and its surroundings. The bottom right inset figure shows the International Container Companies and the ports, and the top right inset figure shows the site location in the scale of Yangtze River Delta (© Google Maps).

.

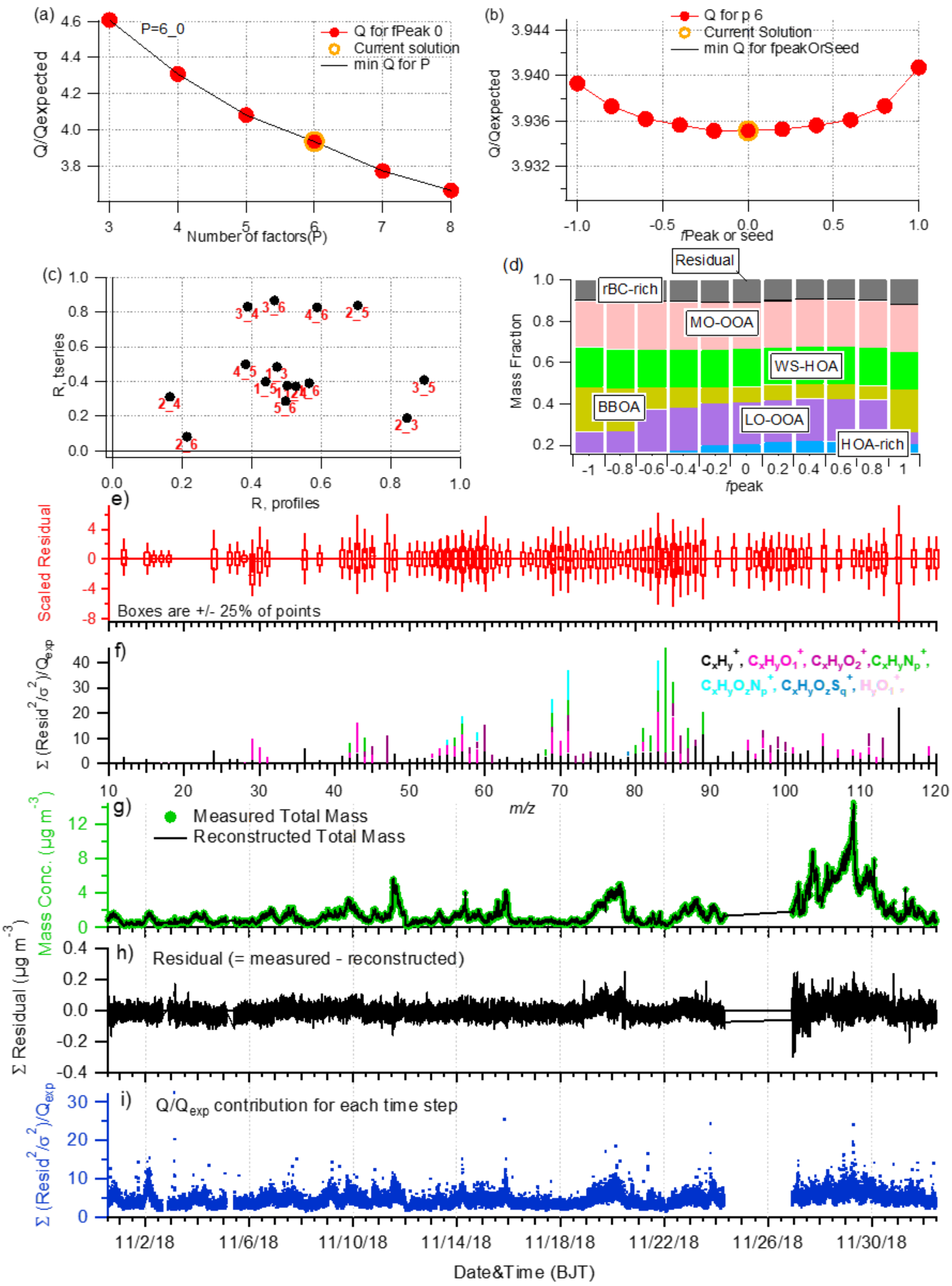

Figure S2. Summary of critical diagnostic plots of the PMF results for the 6-factor solution of *r*BCc OA: (a) Q/Q_{exp} as a function of the number of factors (P from 3 to 8). For the beat solution (6-factor): (b) Q/Q_{exp} as a function of *f*Peak, (c) cross-correlations of the time series and spectral profiles among the six factors, (d) fractions of OA factors as a function of *f*Peak, (e) the box and whiskers plot showing the distributions of scaled residuals for each *m/z*, (f) the Q/Q_{exp} values for each ion, (g) time series of the measured and the reconstructed OA mass loadings, (h) variations of the residuals of the fit, (i) the Q/Q_{exp} values for each time step.

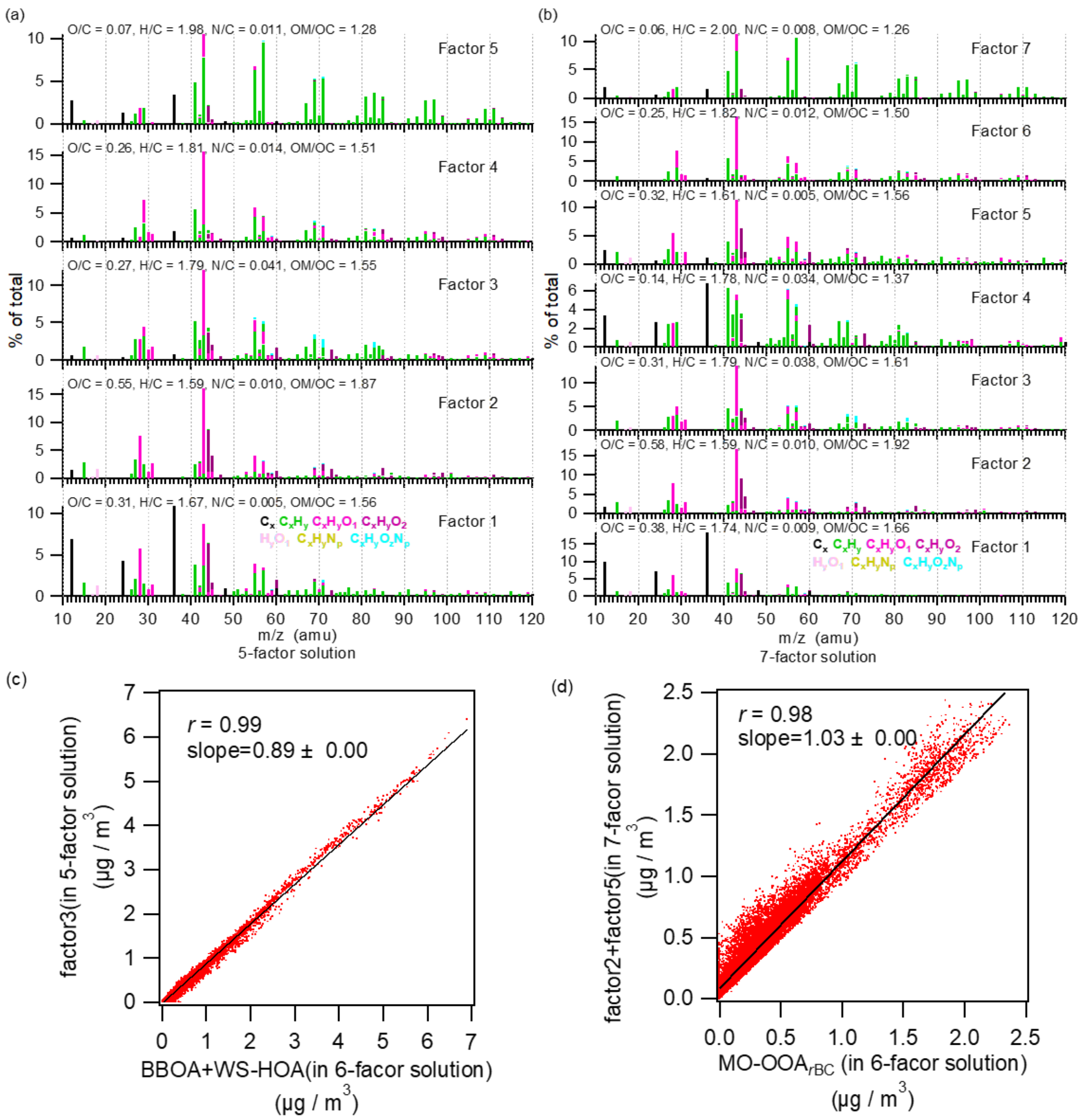

Figure S3. The average mass spectra of (a) 5-factor solution (factor 3 was a mixed factor of BBOA and WS-HOA) and (b) 7-factor solution (MO-OOA splits into two factors, factor 5 and factor 2) resolved from positive matrix factorization of NR-PM$_1$ OA. Scatter plots of (c) the sum of BBOA and WS-HOA with factor 3 (in 5-factor solution), and (d) the sum of factor 5 and factor 2(in 7-factor solution) with MO-OOA$_{rBC}$.

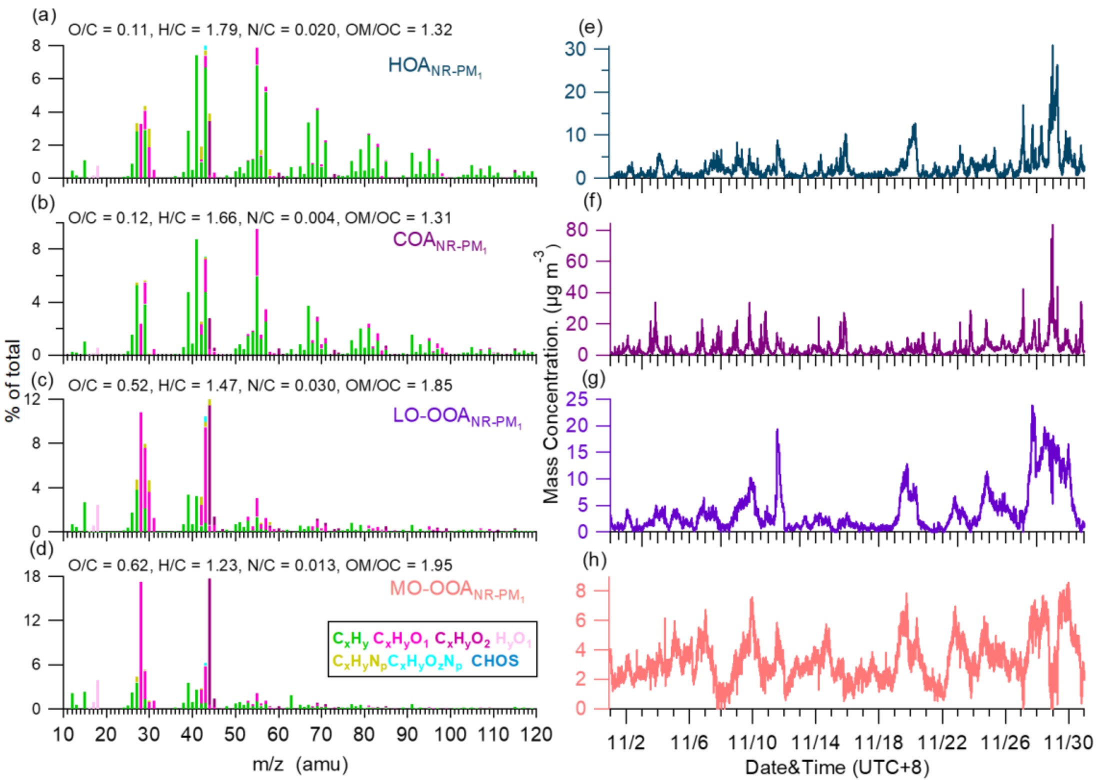

Figure S4. High resolution mass spectra (a-d) and time series (e-h) of the 4-factor solution resolved from PMF analysis of the NR-PM_1 OA.

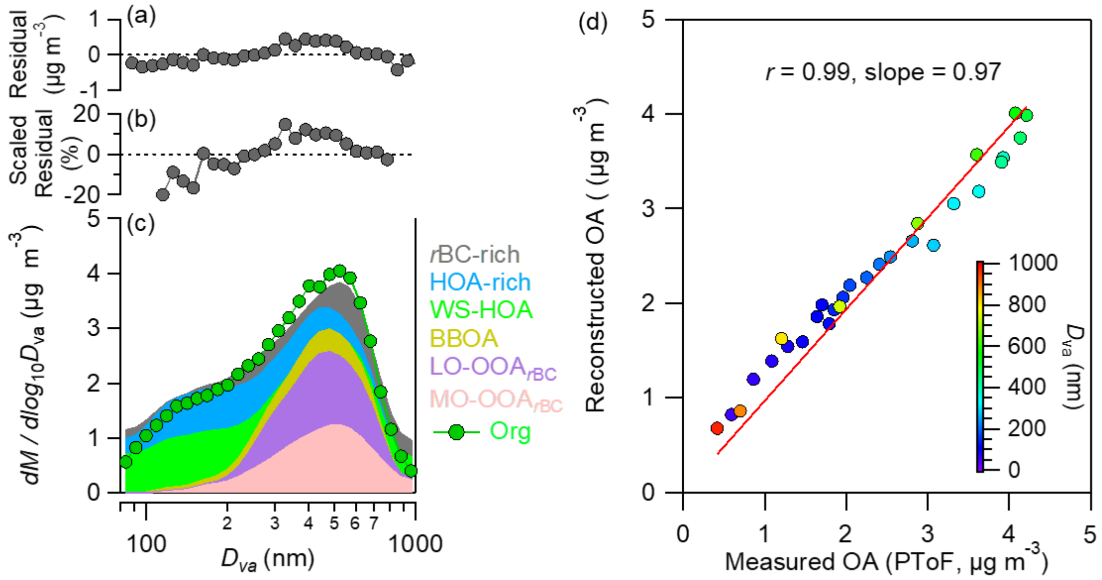

Figure S5. Summary of key diagnostic plots of derivation of size distributions of individual *r*BCc OA factors. (a) Absolute and (b) relative residuals between the reconstructed and measured OA mass concentrations in different size bins. (c) Stacked size distributions of the six OA factors compared to the size distributions of total OA. (d) Reconstructed OA mass concentrations compared to the measured values for different size bins (80-1000 nm).

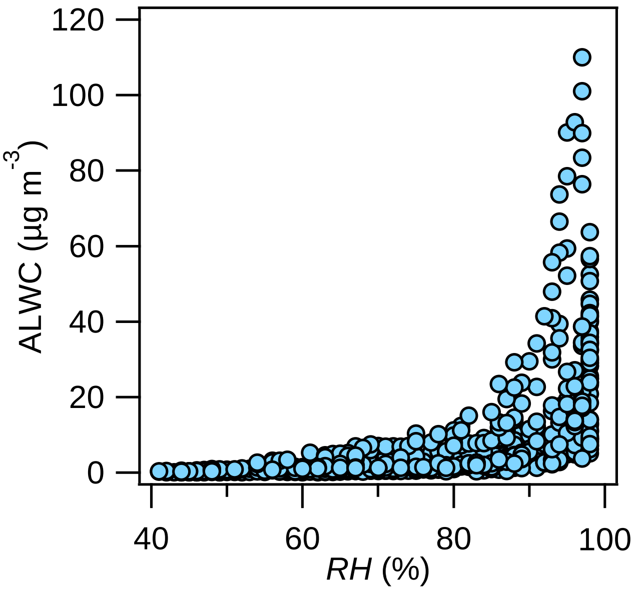

Figure S6. Calculated aerosol liquid water content (ALWC) values versus RH for each time point (see main text for details). The ALWC was calculated by using model II of extended aerosol inorganic model (E-AIM II), and based only on the inorganic components measured by SP-AMS. The main calculation steps are summarized below: (1) the model II determines the state of a system containing water and the inorganic salts in equilibrium at the corresponding temperature and relative humidity (converted to a value of 0-1); (2) the molar concentration of H^+ is obtained according to the ion balance based on the inorganics (SO_4^{2-}, NO_3^- and NH_4^+) measured by SP-AMS (Cl^- is not considered here as it is a very minor component), and the quantities of these four ions (SO_4^{2-}, NO_3^-, NH_4^+ and H^+) are converted to the molar concentrations in particles in per m^3 of air; (3) select the solids allowed to be formed according to the actual condition; (4) use these parameters (temperature, relative humidity, four ions, and allowed solids) to perform the LWC calculations using E-AIM II (http://www.aim.env.uea.ac.uk/aim/model2/model2a.php) online.

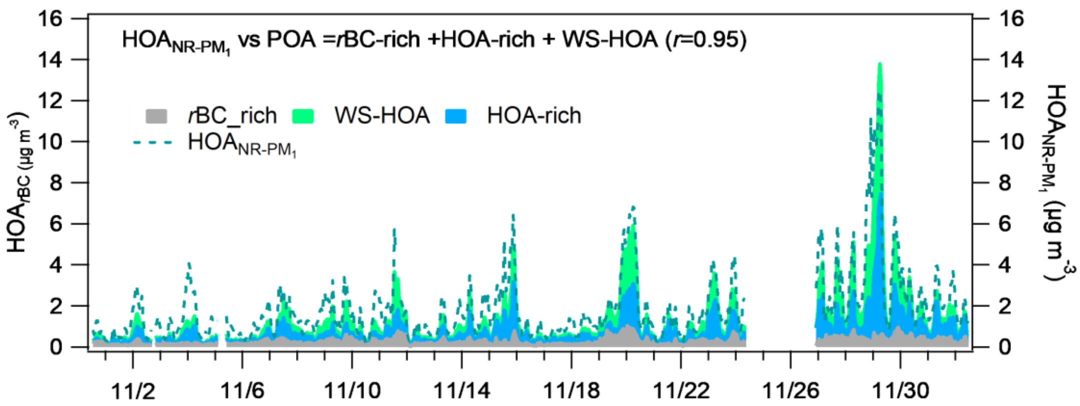

Figure S7. Time series of the stacked three *r*BCc POA factors (termed POA) (i.e., *r*BC-rich, HOA-rich, and WS-HOA) and $HOA_{NR\text{-}PM1}$.

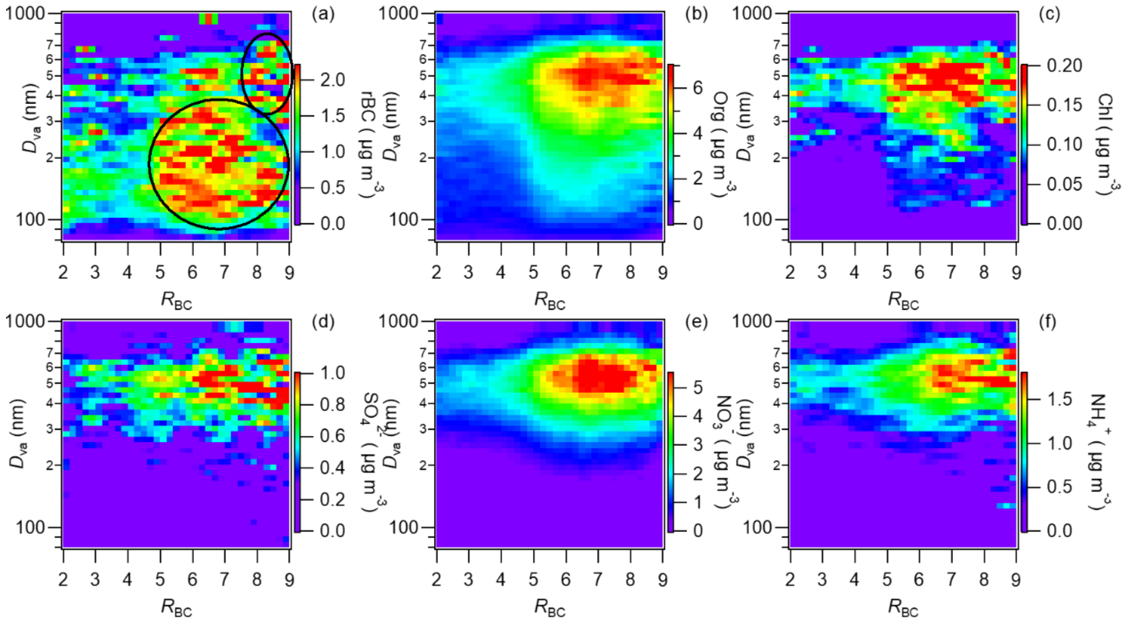

Figure S8. Image plots of size distributions of *r*BCc components as a function of R_{BC}.

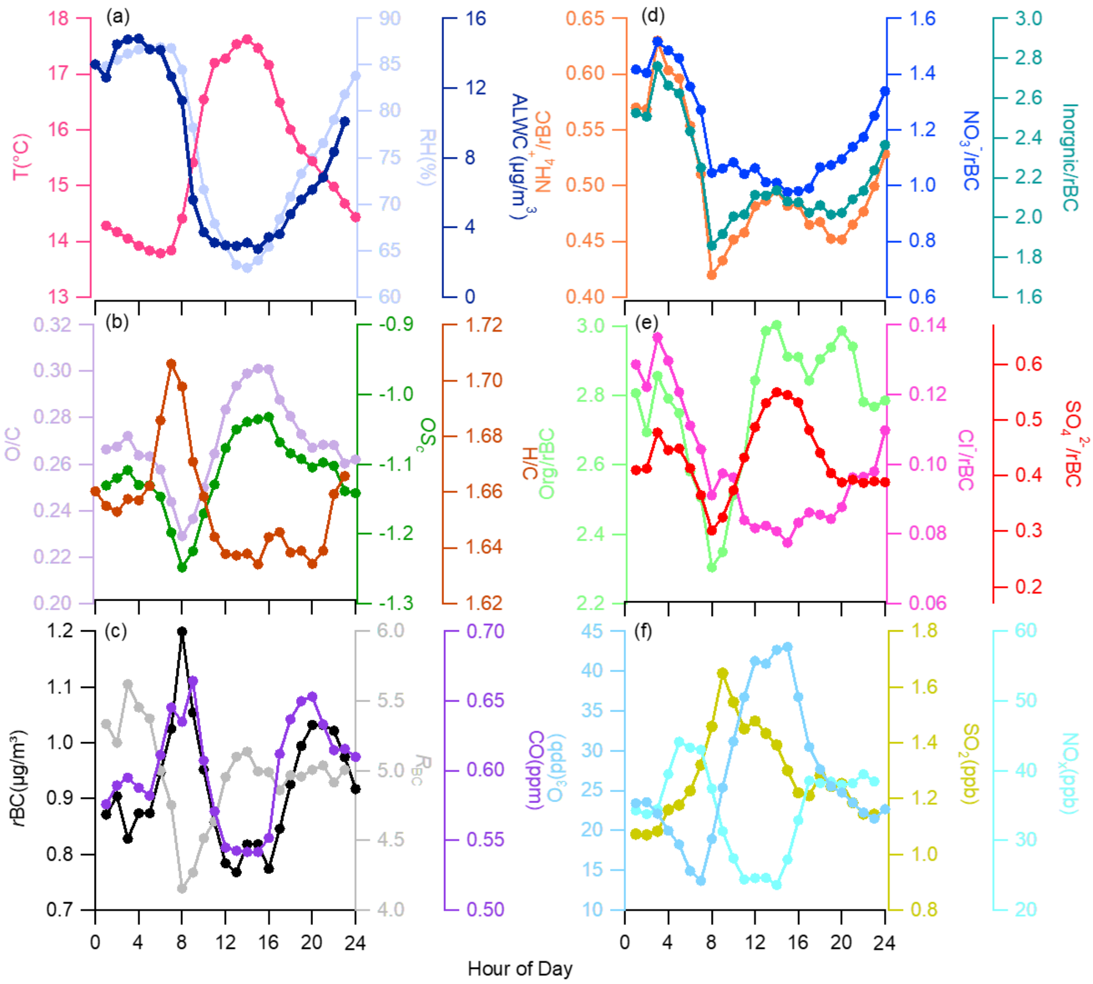

Figure S9. Campaign-average diurnal variations of (a) T, RH and ALWC, (b) O/C, H/C and oxidation state ($OS_C = 2\times O/C - H/C$), (c) R_{BC}, *r*BC and CO, (d) NO_3^-/*r*BC, NH_4^+/*r*BC and inorganics/*r*BC (inorganics=$NO_3^- + NH_4^+ + SO_4^{2-} + Cl^-$), (e) SO_4^{2-}/*r*BC, Cl^-/*r*BC and organics/*r*BC, and (f) gaseous species (O_3, SO_2, NO_X).

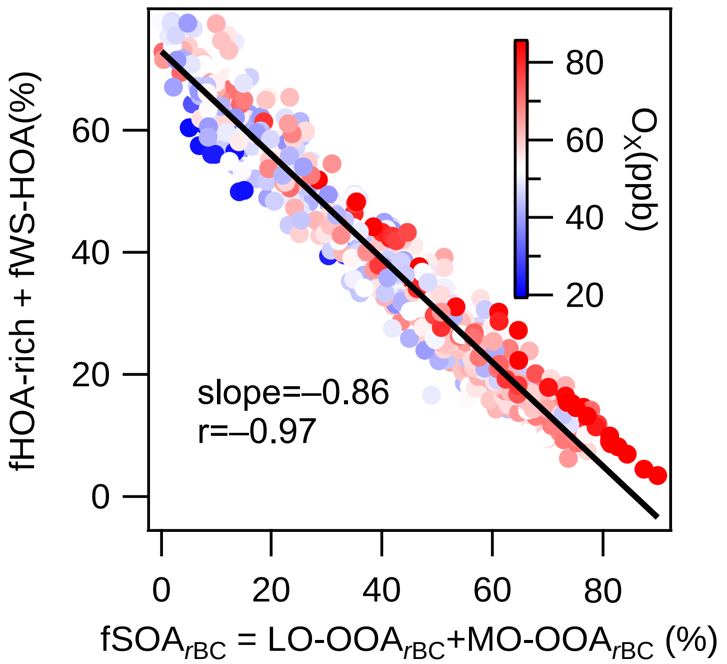

Figure S10. Relationship between the mass fraction (%) of the sum of HOA-rich and WS-HOA and the sum of LO-OOA$_{rBC}$ and MO-OOA$_{rBC}$) (colored by O_X concentrations).

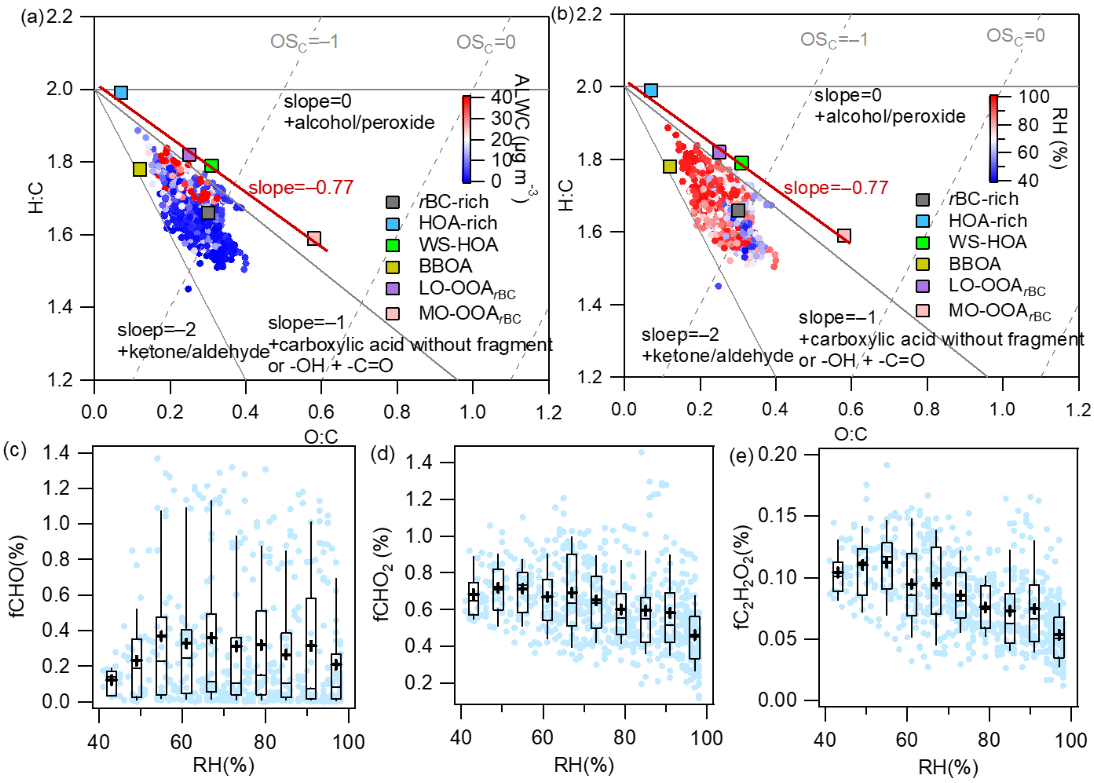

Figure S11. Van Krevelen diagram of H/C versus O/C ratios for all *r*BCc OA and the six factors colored by ALWC (a) and RH (b) (the red line is the fitted line of the four OA factors). (c-e) Mass fractions of selected oxygenated ion fragments as a function of RH (the whiskers above and below the boxes mark the 90% and 10% percentiles, respectively; the upper and lower edge of the boxes represent the 75% and 25% percentiles, respectively; and the lines and triangles inside the boxes denote the median and mean values, respectively).

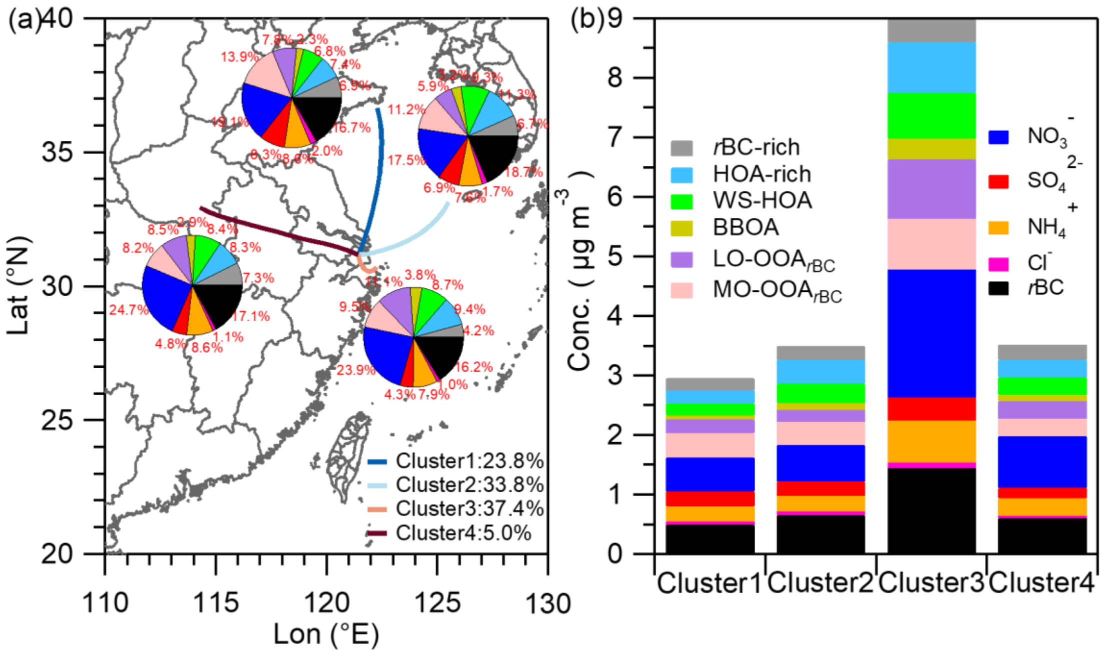

Figure S12. (a) Four clusters of 24-h backward trajectories (at altitude of 500 m) analyzed by NOAA HYSPLIT model (http://www.arl.noaa.gov/ready/hysplit4.html) embedded in Zefir(Petit et al., 2017), with the pie chart showing the average *r*BCc chemical compositions in each cluster. (b) Stacked mass concentrations of the *r*BCc components of the four clusters.

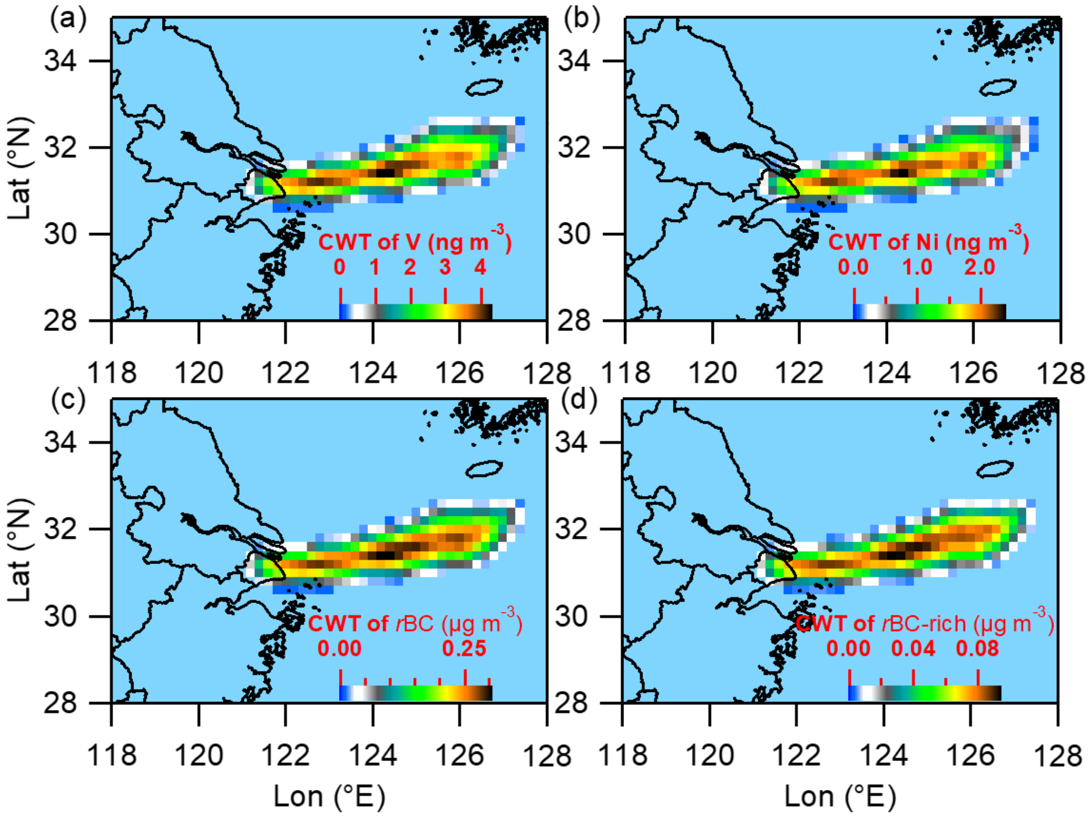

Figure S13. Concentration-weighted trajectories (CWT) of ship emission tracers of V (a) and Ni (b), and *r*BC (c) and *r*BC-rich OA factors (d) (the regions with high CWT values indicate potentially high concentrations of these species).

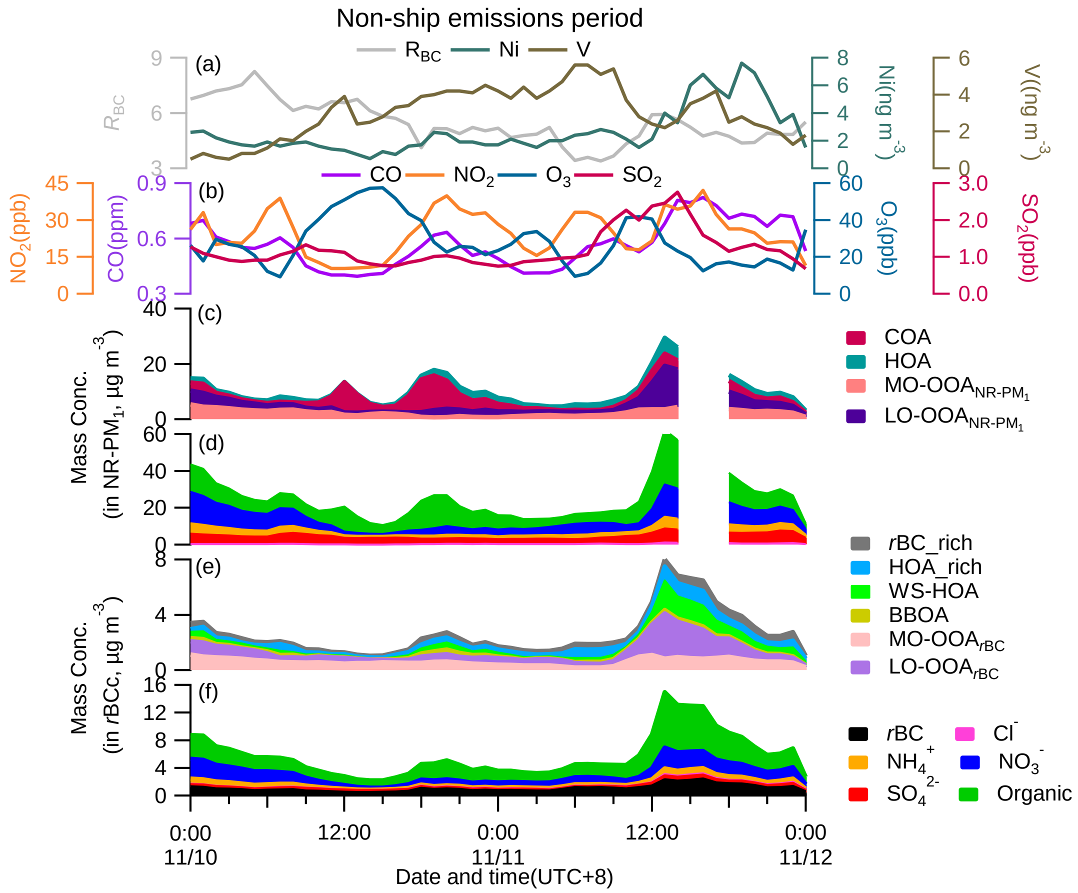

Figure S14. Time series of (a) mass concentrations of particle-phase Ni and V, and R_{BC}, (b) mass concentrations of CO, NO_2, O_3, SO_2, stacked concentrations of (c) NR-PM_1 OA factors, (d) NR-PM_1 species, (e) *r*BCc OA factors, and (f) *r*BCc components during the non-ship emission period (Non-SEP).

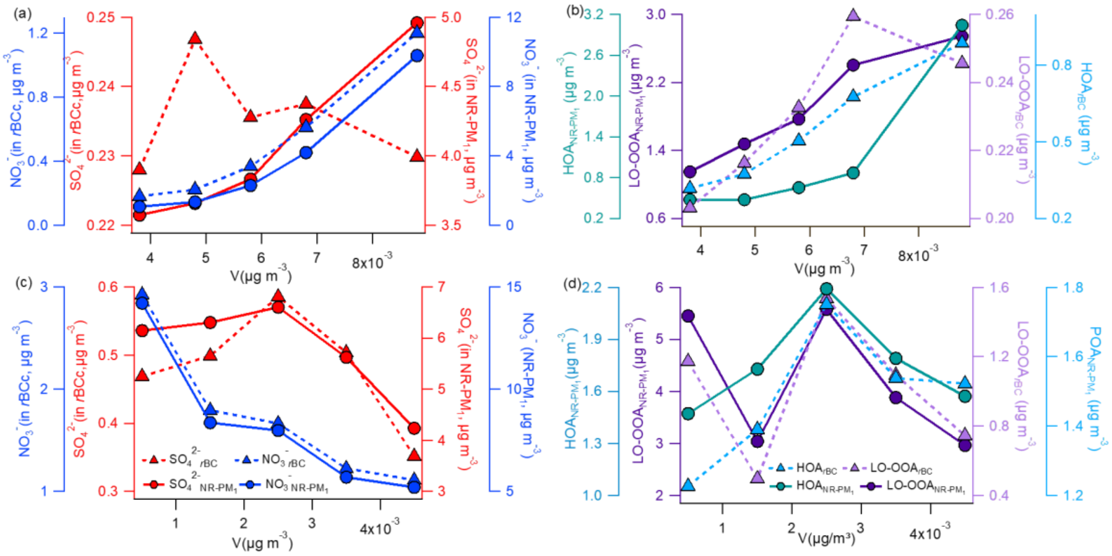

Figure S15. Mass concentrations of the *r*BCc nitrate, sulfate, OA factors in *r*BCc (dashed lines) and in NR-PM$_1$ (solid lines) as a function of V concentrations during ship emission period (a, b) and non-ship emission period (c, d).

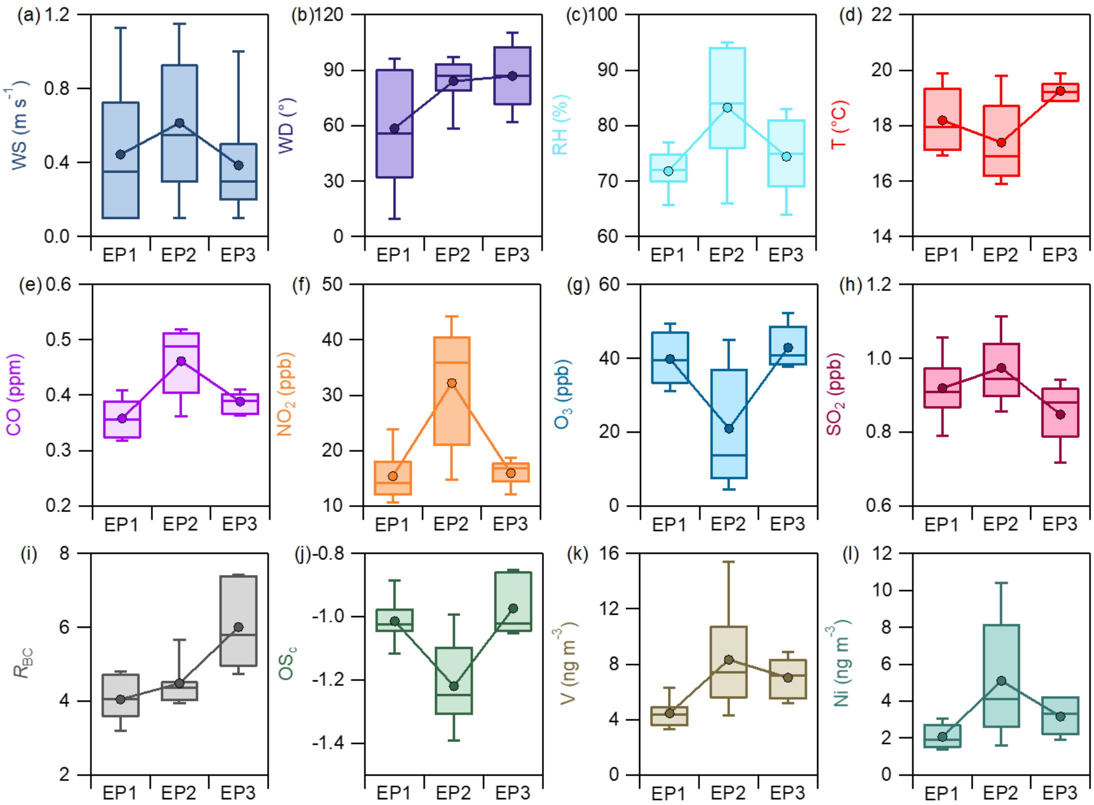

Figure S16. Box plots of meteorological parameters (a-d), gaseous pollutants (e-h), R_{BC} (i), OS_C (j), and ship emission tracers V (k) and Ni (l) of the three episodes during ship emission period (SEP)(meanings of the boxes are the same as those described in Fig. S8).

References

Chang, R. Y. W., Slowik, J. G., Shantz, N. C., Vlasenko, A., Liggio, J., Sjostedt, S. J., Leaitch, W. R., and Abbatt, J. P. D.: The hygroscopicity parameter (κ) of ambient organic aerosol at a field site subject to biogenic and anthropogenic influences: relationship to degree of aerosol oxidation, Atmos. Chem. Phys., 10, 5047-5064, https://doi.org/10.5194/acp-10-5047-2010, 2010.

Gysel, M., Crosier, J., Topping, D. O., Whitehead, J. D., Bower, K. N., Cubison, M. J., Williams, P. I., Flynn, M. J., McFiggans, G. B., and Coe, H.: Closure study between chemical composition and hygroscopic growth of aerosol particles during TORCH2, Atmos. Chem. Phys., 7, 6131-6144, https://doi.org/10.5194/acp-7-6131-2007, 2007.

Wu, Z. J., Zheng, J., Shang, D. J., Du, Z. F., Wu, Y. S., Zeng, L. M., Wiedensohler, A., and Hu, M.: Particle hygroscopicity and its link to chemical composition in the urban atmosphere of Beijing, China, during summertime, Atmos. Chem. Phys., 16, 1123-1138, https://doi.org/10.5194/acp-16-1123-2016, 2016.